JOURNAL OF COMPUTATIONAL PHYSICS **125,** 395–402 (1996)
ARTICLE NO. 0101

A Spectral Method for the Equal Width Equation

BOSCO GARCÍA-ARCHILLA*

Departmento de Matemática Aplicada y Computación, Universidad de Valladolid, Valladolid, Spain

Received July 8, 1994; revised March 14, 1995

A spectral discretization of the equal width equation (EWE) is presented. The method is shown to be convergent and nonlinearly stable. Time-stepping is performed with high-order Adams methods. The spectral accuracy of the scheme reveals some features of the EWE that the methods previously used could not bare out properly. For instance, we may now study the changes in amplitude and velocity of solitary waves after collisions. © 1996 Academic Press, Inc.

1. INTRODUCTION

The equal width equation (EWE)

$$u_t + uu_x - \delta u_{xxt} = 0, \quad -\infty < x < \infty, t \geq 0, \tag{1}$$

with δ a positive parameter, was introduced by Morrison *et al.* [13] as a model for nonlinear dispersive waves. The EWE represents an alternative to the better known Korteweg–de Vries (KdV) equation and the regularized long wave (RLW) equation. These three model equations possess solitary wave solutions that travel with constant velocity without changing shape.

Few analytical solutions of the EWE are known. In fact, results by Olver [15] show that, unlike the KdV equation, no inverse-scattering theory can exist for the EWE, so that there is little hope of obtaining analytical expressions of the solutions. Numerical methods are then a useful tool for the study of the EWE.

Numerical investigations of the EWE have been presented in [8, 9, 13]. For the RLW equation, a wider numerical experience is available [2, 3–5, 8, 13] and the references therein. In most of these papers, finite differences or finite elements are used for spatial discretization and a low-order method for time integration. In the present paper, a method is proposed for the numerical solution of the EWE. The method uses spectral Fourier discretization in space, which yields high accuracy at a fraction of the cost of previously used methods. For the time integration, a high-order multistep code is employed, so that the high accuracy of the spatial discretization (global errors in the range 10^{-9}–10^{-11}) is maintained while allowing for large stepsizes.

We show that the method is nonlinearly stable and convergent with arbitrarily high order. Although for simplicity we treat only the EWE, both the numerical method and the analysis may be straightforwardly extended to the RLW equation.

We present numerical experiments with solitary wave collisions. The accuracy of the method allows us to clearly observe changes in the amplitude and velocity of the interacting waves. These changes agree with similar observations in numerical tests with the RLW equation by Bona *et al.* [4]. However, according to the authors, the accuracy of the numerical method used in [4] was not enough to ascertain whether the observed changes were due to discretization errors or to the true dynamics of the equation.

The efficiency (i.e., high accuracy at low computational cost) of the numerical scheme presented here is also useful when investigating some fine details of the EWE.

The rest of the paper is as follows. Section 2 summarizes some properties of the EWE. In Section 3 the numerical method is described and analyzed. Section 4 is devoted to numerical experiments and, finally, Section 5 contains the conclusions.

2. THE EQUATION

Morrison *et al.* [13] show that in the EWE the quantities

$$C1 = \int_{-\infty}^{\infty} u(x)\, dx,$$

$$C2 = \int_{-\infty}^{\infty} (u^2(x) + \delta u_x^2(x))\, dx,$$

$$C3 = \int_{-\infty}^{\infty} u^3(x)\, dx,$$

remain constant in time. Furthermore, these are the only polynomial invariants of the equation. Notice that the conservation of $C2$ implies that the norm in H^1 is bounded in time. Here and later, for $m \geq 1$, H^m denotes the space of functions with m square-integrable derivatives, and $\|\cdot\|_m$

* E-mail: bosco@mac.cie.uva.es. Current address: Departamento de Matemáticas, Universidad Autónoma de Madrid, 28049 Madrid, Spain.

0021-9991/96 $18.00

the corresponding norm $\|u\|_m = (\|u\|^2 + \cdots + \|u^{(m)}\|^2)^{1/2}$, where in turn $\|\cdot\|$ stands for the standard L_2 norm with the associated inner product

$$(u, v) = \int_{-\infty}^{\infty} u(x)v(x)\,dx$$

(i.e., $\|u\| = (u, u)^{1/2}$). Also, we will be using the maximum norm $\|u\|_\infty = \sup_{-\infty\le x\le\infty} |u(x)|$, and the fact that every function u in H_1 is continuous, with $u(x) \to 0$ as $x \to \pm\infty$, and satisfies

$$\|u\|_\infty \le C\,\|u\|_1 \tag{2}$$

for a positive constant C (see [19, Section 6]).

The EWE possesses solitary wave solutions of the form

$$u(x, t) = 3A\,\mathrm{sech}^2\left(\frac{1}{2\sqrt{\delta}}(x - x_0 - At)\right), \tag{3}$$

with A a constant. The function (3) corresponds to a wave of amplitude $3A$, initially centered at x_0 moving with constant velocity A. Notice that unlike the KdV or RLW equations, the width of the wave does not depend on A and, hence, all solitary waves have the same width.

From the numerical point of view, the most significant property of the EWE is that, when written as an abstract ordinary differential equation in H^1, it possesses a Lipschitz constant. This makes most numerical methods, even explicit methods, unconditionally stable (i.e., stable with no restriction between the time and space steplengths).

In order to check the existence of a Lipschitz constant we write the EWE as

$$u_t = F(u) = -(I - \delta\partial_{xx})^{-1}uu_x. \tag{4}$$

Let u and v functions in H^1 and set $z = F(u) - F(v)$, so that

$$z - \delta z_{xx} = -(uu_x - vv_x).$$

Multiplying by z and integrating, we get, after integration by parts,

$$\|z\|^2 + \delta\|z_x\|^2 = \tfrac{1}{2}((u + v)z, z_x).$$

But

$$\begin{aligned}|((u + v)z, z_x)| &\le \|u + v\|_\infty \int_{-\infty}^{\infty} |z|\,|z_x|\,dx\\ &\le \|u + v\|_\infty\,\|z\|\,\|z_x\|,\end{aligned}$$

and, recalling (2), the last expression is bounded by $C\|u + v\|_1\,\|z\|_1\,\|z_x\|/2$. Hence, if $\|u\|_1, \|v\|_1 \le M$, then

$$\|F(u) - F(v)\|_1 \le \frac{1}{\boldsymbol{\delta}}\sqrt{CM}\,\|u - v\|_1,$$

with $\boldsymbol{\delta} = \min(1, \delta)$. Thus, F is Lipschitz-continuous in bounded sets. In fact, F possess an H^m-Lipschitz constant $L(m)$ in bounded sets in H^m.

Finally, it must be pointed out that by using energy arguments, it is not difficult to prove that if the initial datum u_0 is in H^m, so is the solution for all positive times, although the norm in H^m of the solution may grow with time. Hence, the regularity of the solution is that of the initial condition.

3. THE NUMERICAL METHOD

3.1. *The Spatial Discretization*

To discretize the EWE we first restrict the equation to finite spatial intervals. To do this, we consider periodic boundary conditions. This is a standard procedure in dealing with wave phenomena. Notice that since we are mainly concerned with solitary waves and these decay exponentially, the error perpetrated when replacing the pure initial value problem by a periodic initial value problem with a sufficiently large spatial interval is negligible. The conservation properties and the existence of a Lipschitz constant of the EWE also hold in the periodic case. Henceforth, we work in the interval $0 \le x \le l$ and with l-periodic functions. The spaces H^m and the norms introduced so far apply (with obvious modifications) to the periodic case.

The discretization in space that we use is the *standard* spectral Fourier method (see, e.g., [6]). Fourier methods have been extensively used in wave problems (see, e.g., [14]). We denote by S_N the space of trigonometric polynomials spanned by $\exp(j(2\pi i/l)x)$, $j = -N/2, \ldots, N/2 - 1$, and by P_N the orthogonal projection of $L^2(0, l)$ onto S_N. For N an even positive integer, the approximation is required to be in S_N, that is,

$$u^N(t, x) = \sum_{j=-N/2}^{N/2-1} \tilde{u}_j(t)\exp\left(j\frac{2\pi i}{l}x\right).$$

For an initial value problem given by (1), together with the initial datum

$$u(x, \cdot) = u_0, \tag{5}$$

the numerical approximation is then given by the solution of

$$u^N_t + P_N(u^N u^N_x) - \delta u^N_{xxt} = 0, \tag{6}$$

$$u^N(0, \cdot) = u^N_0, \tag{7}$$

where the initial condition u_0^N is chosen as a suitable representation in S_N of the initial condition u_0 in (5). In our experiments $u_0^N = I_N(u_0)$, the trigonometric interpolant of u_0 based on nodes 0, l/N, ..., $l - l/N$ [6 p. 39].

The discretization (6) has several properties. First, multiplication by 1, u^N, and $(u^N)^2$ and integration by parts leads to the same conservation laws as in the continuous case. Notice then that the norm in H^1 of u^N is bounded for all times. In particular this implies that the L^2 norm of the numerical solution cannot grow without control as time evolves. This is sometimes (wrongly) referred to as stability.

The scheme, however, is truly (nonlinearly) stable. To show this, we rewrite (6) as

$$u_t^N = F_N(u^N) = -(I - \delta\partial_{xx})^{-1} P_N u^N u_x^N, \tag{8}$$

from which it is clear that the discretization possesses the same Lipschitz constant $L = \sqrt{CM}/\boldsymbol{\delta}$ as F in (4). Stability is now easily proved. Fix $T > 0$ and let v^N, w^N: $[0, T] \to S_N$ satisfy $\|v^N(t)\|_1$, $\|w^N(t)\|_1 \le M$, $t \in [0, T]$. We have that

$$v_t^N + (I - \delta\partial_{xx})^{-1} P_N v^N v_x^N = (I - \delta\partial_{xx})^{-1} f^N,$$
$$w_t^N + (I - \delta\partial_{xx})^{-1} P_N w^N w_x^N = (I - \delta\partial_{xx})^{-1} g^N,$$

for certain residuals f^N and g^N. Subtracting these equations and taking norms, from Gronwall's lemma then stability follows, in the sense that

$$\|e^N(t)\|_1^2 \le e^{LT}(\|e^N(0)\|_1^2 + T \max_{0\le t\le T} \|f^N(t) - g^N(t)\|^2), \quad 0 \le t \le T, \tag{9}$$

where $e^N = v^N - w^N$. This, besides allowing us to prove convergence, ensures that the method has good numerical properties [17].

Convergence can be proved in the standard way. Replace v^N by the numerical solution u^N of (6)–(7) and w^N by the projection $P_N u$ of the true solution. The corresponding residuals are then $f^N = 0$ and $g^N = T^N$, where T^N is the truncation error

$$\begin{aligned} T^N &= P_N u_t + P_N(P_N u P_N u_x) + P_N u_{xxt} \\ &= P_N \tfrac{1}{2}((u - P_N u)(u_x + P_N u_x) \\ &\quad + (u + P_N u)(u_x - P_N u_x)). \end{aligned} \tag{10}$$

Here, we have used that $(P_N u)_x = P_N u_x$. Taking norms in (10) and using the well-known fact (see, e.g., [6 pp. 278–279]) that for $v \in H^m$,

$$\|I_N(v) - v\|_k \le C(m) N^{k-m} \|v\|_m, \quad k = 0, 1, ..., m - 1, \tag{11}$$
$$\|P_N(v) - v\|_k \le C(m) N^{k-m} \|v\|_m, \quad k = 0, 1, .., m - 1, \tag{12}$$

it is easily checked that $\|T^N\| = O(N^{-m+1})$ if the initial condition u_0 (and consequently u) is in H^m. This, together with the stability (9) and (11), show convergence of order $m - 1$ (i.e., $\|u^N - u\|_1 = O(N^{m-1})$), which implies convergence of arbitrary high order for analytical u. In fact, for analytical v, the constant C in (11)–(12) can be replaced [18] by $C(\nu)e^{-\nu N}$ for some positive ν, so that the method is exponentially convergent.

Notice that, for all these arguments to be valid both the true solution u and the numerical solution u^N must be bounded in H^1, but that this is ensured by the conservation of $C2$.

3.2. *The Time Integration*

In terms of the coefficients $\tilde{u}^N = (\tilde{u}_{-N/2}, ..., \tilde{u}_{N/2-1})^T$ of u^N, (8) (or (6)) becomes the system of ordinary differential equations (ODEs)

$$\frac{d\tilde{u}^N}{dt} = (I - \delta D_2)^{-1} D_1 \tfrac{1}{2}\widetilde{(u^N)^2}, \tag{13}$$

where D_1 and D_2 are diagonal matrices with entries $2\pi ij/l$ and $-4\pi^2 j^2/l^2$, respectively. In order to maintain the high spatial resolution provided by spectral discretizations, either very small time stepsizes or high-order time integrators are needed. The first alternative usually makes the computation of the solution prohibitively expensive, so we use high-order methods. Typically, the system of ODEs obtained by discretizations of PDEs are stiff; that is, they have Lipschitz constants that are large with respect to the rate of change of the solutions. For many PDEs the Lipschitz constant of the induced systems of ODEs grows like a power of the number of degrees of freedom N. Stiffness usually makes time integration costly and difficult to handle. In the PDE framework, stiffness is responsible for the impossibility of explicit methods being unconditionally stable.

The existence of a Lipschitz constant independently of N in (6), (8) allows the use of nonstiff ODE solvers. This way of carrying out the time integration is quite an exception in PDEs and is restricted to a few equations like the EWE and RLW equations and, in general, to equations of the Sobolev type [7]. High-order methods have been used in the time integration of the RLW equation. In [2] the authors use one of the "black-box" routines of the IMSL library, with an implementation of an extrapolation method. More recently, however, it has become apparent that extrapolation methods are in general less cost-effective than other methods like those used in [3–5]. In fact, Hairer *et al.* [10, Section II.10] show that extrapolation methods only become effective when the errors desired are below 10^{-13}. For the accuracy we achieve in this paper, Adams formulae or high-order pairs of embedded Runge–

Kutta (RK) methods like RK7(8) and DOPRI8 [10, pp. 194–195] are better suited from the efficiency point of view.

The right-hand side in (13) can be evaluated by collocation and fast Fourier transform (FFT) [6, pp. 38, 85], in less than $(\frac{15}{4}\log_2(3N/2) + \frac{3}{2})N$ flops; that is, its cost is almost proportional to the dimension of (13). This makes RK methods a better choice than multistep methods [10, pp. 379–380]. However, we used in our experiments a variable-stepsize variable-order implementation of the Adams multistep methods, with orders up to 12, since we were also interested in studying other (not reported here) numerical phenomena. Also for this reason, we programmed the code ourselves. To write the code, we followed suggestions in [10, Sections III.5, III.7; 12, Section 4.4]. Using variable-stepsize, variable-order Adams methods in wave problems are not new [16], although their computational advantages are limited unless, as in the present case, the PDE to be integrated possesses a Lipschitz constant [11].

4. NUMERICAL EXPERIMENTS

In this section, we present only those numerical experiments whose outcome add significantly to the extensive tests reported in [9]. The experiments were carried out on a Sun SPARC Station 10/40. The numerical method was programmed in FORTRAN and for the FFT the NAG library was used.

It may be worth first commenting on the capabilities of the numerical method presented in this paper. For this purpose, we will compare some results with those obtained by Gardner and Gardner in [9]. The numerical scheme in [9] is a finite element method based on cubic splines. The time integration is carried out by the implicit mid-point rule. The method is then convergent of order 4 in space and order 2 in time.

Let us look at the solution of (1) with $\delta = 1$ and initial condition

$$u_0(x) = 3\,\mathrm{sech}^2\left(\frac{1}{2\sqrt{\delta}}(x-40)\right).$$

This corresponds to a solitary wave of height 3 and moving to the right with velocity 1 (i.e., $A = 1$ in (3)). Gardner and Gardner [9] integrate this problem using 400 elements of length 0.2 in a (spatial) interval of length 80, and with a time step of 0.1 up to time $T = 40$, obtaining an error of 2.52×10^{-2} in the L^2 norm. We compare this result with what was obtained by the method in the present paper at a similar cost. From its description in [8], the cost of the method in [9] can be estimated at 51 × number of elements × number of steps flops, which, for the present experiment, makes a total of 8.1×10^6 flops. A similar figure, 7.6×10^6 flops, was obtained by our method with $N = 180$ (in the spatial interval [0, 120]) and a tolerance (below which local errors are wanted) of 10^{-7}, for which it required 219 steps (most of them with $k = 10$) to complete time integration. The error obtained was 2.57×10^{-5}. Hence, in this example, our method, while being roughly equally costly as that in [9], is about 1000 times more accurate.

TABLE I

Convergence Table for the Single Solitary Wave at $t = 40$

N	$\|E\|$	$\|E\|_\infty$	TOL	Steps	CPU time
120	5.57E-3	2.01E-3	1E-06	178	4.750
180	5.76E-5	1.76E-5	1E-08	274	11.03
240	5.53E-7	1.64E-7	1E-10	409	21.24
300	5.01E-9	1.52E-9	1E-11	479	28.40

In Table I (left-most four columns) the errors for the present method are shown for different values of N. For each value of N, the tolerance with which the method was run was the largest one for which the errors arising from spatial discretization dominate over those arising from the time integrator. The corresponding tolerances, number of steps, and CPU times are shown in the three leftmost columns of Table I. Notice how doubling N from 120 to 240 reduces the error by a factor of 10000. This is typical of spectral methods [6, p. 6]. However, the cost is multiplied only by 5. A similar reduction in the error with the method in [9] would mean increasing the cost by a factor of 1000. Notice also that the efficiency of our method is achieved by the combination the spatial discretization and the time integrator. Had we used the same time integrator as in [9], reducing the error by 10000 would have meant increasing the cost by a factor of 200 instead of 5.

In the rest of the experiments reported in this paper, the tolerance used was 10^{-11}. The length l of the spatial interval was always chosen so that $u_0(l)$ and $u_0(0)$ were of the order of 10^{-16}, and the number of modes N was chosen so that the coefficient $\tilde{u}_N$ times $\sqrt{N}$ was also around 10^{-16}. Hence the initial data is reproduced as accurately as possible.

Experiment A (Interaction of two positive waves). The first question we address is the interaction of two positive waves of different amplitude (and hence different velocities). The initial condition we used for (1) with $\delta = 1$ was

$$u_0(x) = 10.2\,\mathrm{sech}^2\left(\tfrac{1}{2}(x-40)\right) + 5.1\,\mathrm{sech}^2\left(\tfrac{1}{2}(x-100)\right)$$

(see Fig. 1a). The taller wave, moving to the right with velocity double (=3.4) that of the smaller wave overtakes this one at time $t = 60/1.7$ and $x = 160$. We simulated this interaction using $N = 1536$ modes in the interval [0, 360].

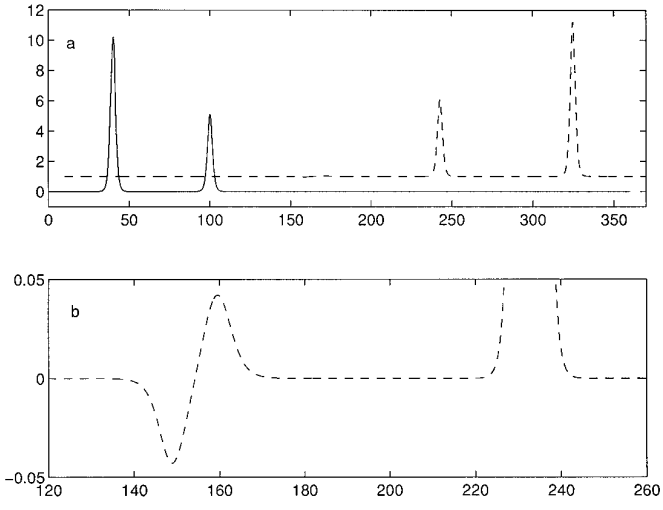

FIG. 1. Interaction of positive waves: (a) solution at ———, $t = 0$; – –, $t = 80$; (b) solution at $t = 80$ (magnified).

Figure 1a shows also the result at time $t = 80$. The solution is also reproduced, in a magnified scale, in Fig. 1b.

The two waves have emerged apparently unchanged but for a phase shift. Also, a pair of two daughter waves of opposite signs have appeared. This is what is reported in [9] for the same experiment.

However, since the quantity $C2$ is conserved and since the daughter waves contribute to the value of $C2$, the emerging large waves cannot be the same as the incoming ones. To check this fact (surprisingly unnoticed in part of the previous literature) we measured the heights and velocities of the waves before and after collision. Before collision the mean values of these heights in the time interval [0, 12] are 10.20000076 and 5.10000038; the relative error with respect to the theoretical values is then below 10^{-7}. After the collision the values are 10.20030499 and 5.09878321; that is, the relative error with respect to the theoretical values is now larger than 2×10^{-5}.

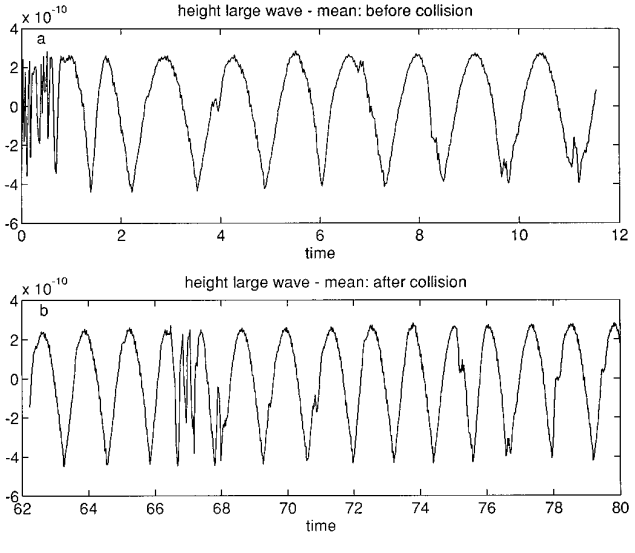

FIG. 2. Height of large wave minus its mean: (a) before collision (mean = 10.20000076); (b) after collision (mean = 10.20030499).

This increase in the departure from theoretical values after collision is not justified in terms of numerics. Figures 2 show that the deviation of the computed heights from their means in the large wave is below 5×10^{-10} both before and after collision and that it does not grow with time. A similar behaviour was found for the smaller wave. Also, the variations of the quantities $C1$, $C2$, and $C3$ were below 10^{-10}. Furthermore, we repeated the experiment with $N = 2048$ and TOL $= 10^{-12}$ and the results differed less than 3×10^{-8}.

We also checked that the computed heights and velocities of the waves are in agreement. The velocities, which were determined by a least squares fit, are 3.400000256 and 1.700000128 before collision and 3.40010169 and 1.69959422 after collision. Notice that they coincide, up to eight significant digits, with one third of the corresponding computed heights.

Bona *et al.* [3], for a similar experiment with the closely related RLW equation, also observed variations of the order of 10^{-5} in the heights of the emerging waves. However, the accuracy of their scheme did not guarantee that the variation was not due to roundoff or discretization error. In our case, the variations observed are well above the errors, so that they can be taken as occurring in the true (i.e., not numerical) solution.

All the data gathered indicate that, after collision, two solitary waves emerge. The larger one possesses greater values of height and velocity than the largest of the incoming waves, whereas the smaller one loses height and velocity with respect to the smallest of the incoming waves; the balance in energy is not maintained, and to compensate for the loss of energy after collision, a pair of daughter waves emerge.

In view of other examples, Gardner and Gardner [9] suggest that a source of solitary waves is created at the site of the encounter. This is not exactly so. Rather, the two daughter waves start moving in opposite directions, creating a sort of rarefaction wave (a fact pointed out in [1]), and, once they are quite apart from each other, the daughter waves decompose in solitary waves. This can be seen in Figs. 3 and 4, where it can be observed how solitary waves emerge from the daughter waves, leaving them behind. The pair of daughter waves, in turn, lose height and speed. Also, this process seem to show some sort of self-similarity behaviour. Figure 4 shows the solution at $t = 3080$. Notice the resemblance of the magnified plot with that in Fig. 3 corresponding to $t = 830$.

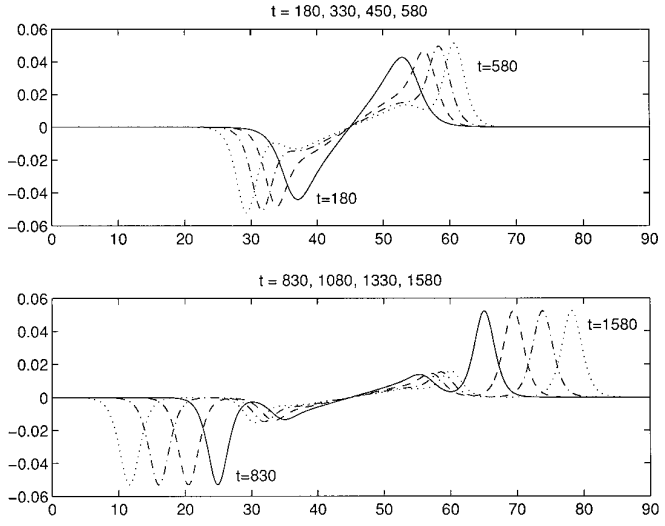

FIG. 3. Interaction of two positive waves; evolution of the daughter waves.

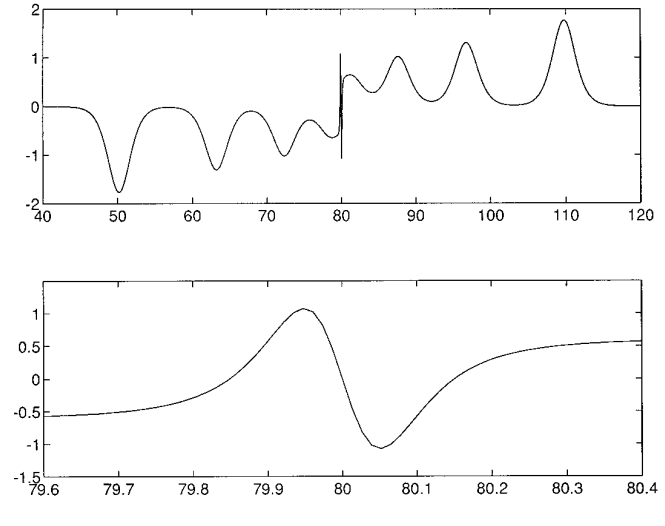

FIG. 5. Interaction of two opposite waves; solution at time $t = 81.6$. Lower plot in magnified scale.

EXPERIMENT (B) (Interaction of opposite waves). Our second issue concerns solitary waves of opposite amplitudes. We used as initial condition

$$u_0(x) = 4.5\,\mathrm{sech}^2(\tfrac{1}{2}(x-40)) - 4.5\,\mathrm{sech}^2(\tfrac{1}{2}(x-120)),$$

which corresponds to two waves of amplitudes 4.5 and -4.5, initially centered at 40 and 120 and moving in opposite directions with velocity 1.5. We solved this problem with $N = 3072$ in the interval [0, 160]. Figure 5 shows the computed solution at time $t = 81$, 20 time-units after the encounter. Notice that four pairs of solitary waves of opposite amplitudes have been generated after the collision. There is also what appears to be a spike at the site of the encounter. On a magnified scale, this spike is seen to be the remains of the original waves.

The interaction of two opposite waves turned out to be a particularly difficult problem. We first noticed this fact when we checked our results agains those of Gardner and Gardner [9]. These authors report that, also 20 time units after collision, the amplitudes of the emerging waves are 1.78, 1.47, 1.36, and 1.15. Our measures are 1.766, 1.308, 1.02, and 0.65. The disagreement would be noticeable even in a plot of the solution.

To check our values, we compared the numerical solution with the result corresponding to $N = 12288$. The infinity norm of the difference between the two solutions was 0.0207, and this maximum was attained at the spike. In the four emerging waves the errors were (from largest to smallest amplitude) less than 10^{-4}, 2×10^{-4}, 7×10^{-4}, and 2×10^{-3}, so that the digits in the values shown above may be taken as correct. Furthermore, in Table II, the errors for different values of N are shown (taking as an exact solution those corresponding to $N = 12288$). Notice how this table differs from Table I, showing that this problem

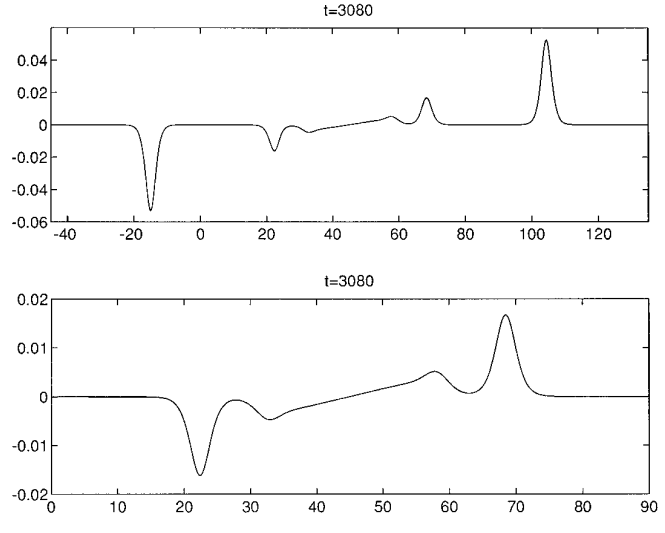

FIG. 4. Interaction of two positive waves; evolution of the daughter waves.

TABLE II

Interaction of Two Opposite Waves: Errors with TOL = 10^{-11}

N	$\|E\|$	$\|E\|_\infty$	CPU time
1024	2.26405	0.92302	219.55
2048	9.32E-2	1.40E-1	488.71
3072	1.40E-2	2.07E-2	776.44
4096	2.23E-3	3.05E-3	1057.1
6144	5.54E-5	6.67E-5	1699.1

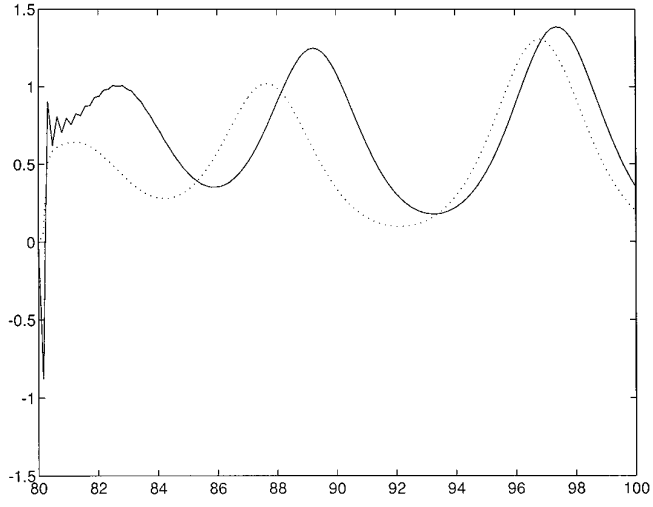

FIG. 6. Interaction of two opposite waves; solution at $t = 81.6$; ———, $N = 1024$; ..., $N = 12288$.

is far more difficult to treat numerically than those treated above.

The plot of the solution corresponding to $N = 1024$ (Fig. 6) is quite revealing. The spike of the true solution is so narrow that the mesh for $N = 1024$ is not fine enough to represent it correctly. This is manifest by the oscillations near $x = 80$ that suggest that the variations in the solution are so large they are interpreted as discontinuities. However, the spatial discretization conserves energy (the invariant $C2$) and the time integrator, although not conservative, keeps $C2$ almost constant (Fig. 7). Hence, the numerical solution must dump energy away from the spike sooner and in larger quantities than the true solution. This results in the formation of larger solitary waves (and, hence, traveling faster) than in the true solution. We guess that this also explains why in [9] the emerging solitary waves have larger amplitudes than here.

Finally we investigated the formation of these solitary waves after the encounter. We let evolve two opposite waves of amplitude 13.5 and velocity 4.5, originally centered at 40 and 120. For this experiment we used $N = 12288$ in the interval [0, 160]. In Fig. 8 it can be seen how the original waves squeeze against each other and the spike begins to be formed as its base decreases faster than its

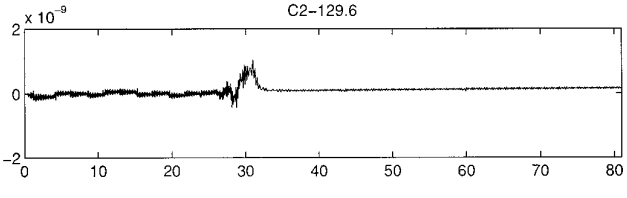

FIG. 7. Interaction of two opposite waves; evolution of $C2$ for $N = 1024$.

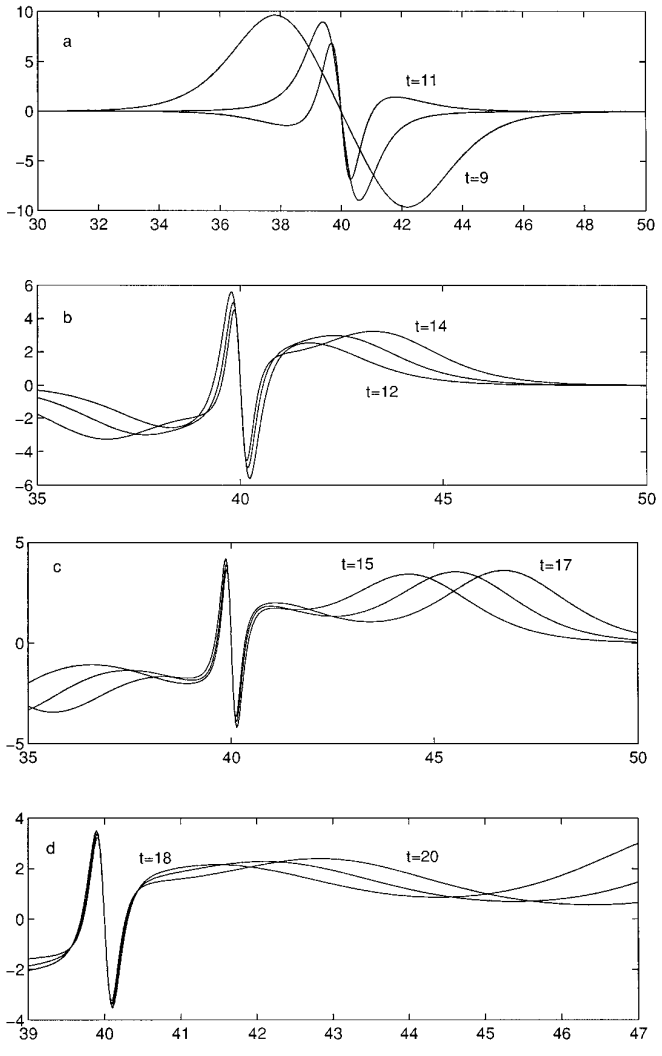

FIG. 8. Interaction of two opposite waves of amplitudes 13.5.

height. At time $t = 11$, energy is being dumped away from the original waves, and at time $t = 14$ a wave begins to separate from the spike that continues to narrow. In Fig. 8c, it can be seen how the newly formed wave leaves the spike, and in Fig. 8d a second wave is formed and begins to detach itself from the spike. Notice the resemblance of Fig. 8d with Fig. 8a which suggests some sort of self-similarity and that this process will continue indefinitely on smaller scales.

5. CONCLUSIONS

A numerical method for the EWE has been introduced and analyzed. The method uses a spectral Fourier discretization for the spatial derivatives, which allows for exponential convergence in the case of analytical solutions. The method is shown to be (nonlinearly) stable and convergent.

Stability follows straightforwardly from the fact that the EWE possesses a Lipschitz constant on bounded sets on H^1.

The existence of a Lipschitz constant in the EWE has been exploited in the time integration of the scheme by using high-order methods for nonstiff ODEs (a feature quite exceptional in PDEs) that allows for great accuracy at a low cost, so that the exponential convergence of the spatial discretization is not ruined by time integration. Examples have been given in which the method is 1000 times more efficient than previously used methods.

The efficiency of the method allows us to study details of the EWE that are hardly observable with previously used methods, and it opens the possibility of an extensive numerical experimentation.

Among the most significant properties of the EWE that the accuracy of the scheme has revealed is the fact that solitary waves do change amplitude and velocity after collisions.

Finally, a detailed study of the collision of opposite waves has shown the numerical difficulties encountered in this simulation. We have also detected the presence of what appears to be phenomena of self-similarity.

ACKNOWLEDGMENTS

This research has been partly financed by DGICYT Project PB92-254. The author is most thankful to Professor Sanz-Serna for a careful reading of the manuscript and for his valuable suggestions.

REFERENCES

1. Kh. O. Abdulloev, I. L. Bogolubsky, and V. G. Makhankov, *Phys. Lett. A* **56,** 427 (1976).
2. M. E. Alexander and J. H. Morris, *J. Comput. Phys.* **30,** 428 (1979).
3. J. L. Bona, W. G. Pritchard, and L. R. Scott, *Phys. Fluids* **23,** 439 (1980).
4. J. L. Bona, W. G. Pritchard, and L. R. Scott, "A Comparison of Solutions of Two Model Equations for Long Waves," in *Lect. Appl. Math.* Vol. 20 (Springer-Verlag, New York/Berlin, 1983), p. 235.
5. J. L. Bona, W. G. Pritchard, and L. R. Scott, *J. Comput. Phys.* **60,** 167 (1985).
6. C. Canuto, M. Y. Hussaini, A. Quarteroni, and T. A. Zang, *Spectral Methods in Fluid Dynamics,* Comput. Phys. (Springer-Verlag, Berlin, 1988).
7. R. Ewing, *SIAM J. Numer. Anal.* **15,** 1125 (1978).
8. L. R. T. Gardner and G. A. Gardner, *J. Comput. Phys.* **91,** 441 (1990).
9. L. R. T. Gardner and G. A. Gardner, *J. Comput. Phys.* **101,** 218 (1992).
10. E. Hairer. S. P. Nørsett, and G. Wanner, *Solving Ordinary Differential Equations I* (Springer-Verlag, Berlin, 1987).
11. E. Hairer and G. Wanner, *Solving Ordinary Differential Equations II* (Springer-Verlag, Berlin, 1991).
12. J. D. Lambert, *Numerical Methods for Ordinary Differential Systems. The Initial Value Problem* (Wiley, Chichester, 1991).
13. P. J. Morrison, J. D. Meiss, and J. R. Cary, *Phys. D* **11,** 324 (1984).
14. F. Z. Nouri and D. M. Sloan, *J. Comput. Phys.* **83,** 324 (1989).
15. P. J. Olver, *Math. Proc. Cambridge Philos. Soc.* **85,** 143 (1979).
16. P. Rosenau and J. M. Hyman, *Phys. Rev. Lett.* **70,** 564 (1993).
17. J. M. Sanz-Serna, "Stability and Convergence in Numerical Analysis I: Linear Problems, a Simple, Comprehensive Account," in *Nonlinear Differential Equations and Applications* edited by J. K. Hale and P. Martínez-Amores (Pitman, London, 1985), p. 64.
18. E. Tadmor, *SIAM J. Numer. Anal.* **13,** 1 (1986).
19. J. Wloka, *Partial Differential Equations* (Cambridge Univ. Press, New York, 1987).